Background-corrected simultaneous multielement atomic absorption spectrometer

ARTICLE · JANUARY 1978

1 AUTHOR:

James Harnly
Agricultural Research Service
163 PUBLICATIONS **3,394** CITATIONS

SEE PROFILE

Background-Corrected Simultaneous Multielement Atomic Absorption Spectrometer

J. M. Harnly and T. C. O'Haver*

University of Maryland, College Park, Maryland 20742

B. Golden and W. R. Wolf

U.S. Department of Agriculture, Nutrient Composition Lab, Beltsville, Maryland 20705

A multielement atomic absorption spectrometer has been developed based on a continuum source and an echelle polychromator modified for wavelength modulation (SIMAAC). The instrument is capable of measuring up to 16 elements simultaneously with either flame or electrothermal atomization. Double beam operation and dynamic background correction are achieved on all channels. Approximately 100 absorbances are calculated per second per channel. Detection limits for SIMAAC with electrothermal atomization are comparable to the single element mode of operation and to commercially available AA instruments using electrothermal atomization.

In recent years there has been considerable interest in the development of multielement atomic spectrometry systems. Most of these have been based on atomic emission or atomic fluorescence measurement; and in fact it has been said that, compared to these methods, atomic absorption is the least likely candidate for multielement development (*1*). Nevertheless, atomic absorption has enjoyed wide acceptance and utilization as a trace element analysis tool both by spectroscopists and by scientists whose main interests are in areas other than spectroscopy itself. As a result, the operating principles, atomization devices, sample preparation and introduction procedures, and potential interferences are already familiar to many users. From this point of view it would seem that a multielement atomic absorption spectrometer has some merit after all. Recently a major manufacturer of atomic absorption instruments has introduced a *sequential* multielement system (*2*) in which elements are measured individually one after the other. This approach, however, does not offer the multiplex advantage of true simultaneous measurement (*1*).

There have been numerous attempts to develop a practical multielement atomic absorption spectrometer (*3–12*). Most of these systems suffer from one or more serious limitations, such as the inability to utilize furnace atomizers, limitations in the number of channels, lack of background correction or double beam operation, or complex constructional requirements. Only three systems have been shown to be able to utilize electrothermal atomization devices. The system of Lundberg and Johansson (*4*) used a carbon rod atomizer and a modified monochromator with three exit slits. Only three elements could be determined simultaneously. Background correction was accomplished by using a continuum source in addition to the multielement hollow cathode lamp. A minicomputer was used for data acquisition and processing. Detection limits were a factor of 2 to 4 higher than those obtained when the same atomizer was used with a commercially available AAS operating in the single element mode. The deterioration of the detection limits was attributed to the time sharing of the data acquisition system, the higher noise and lower intensity of the multielement hollow cathode lamp, and "constructional compromises."

Salin and Ingle (*5*) developed a similar system with a modified, multiexit slit monochromator. Their instrument was restricted to the simultaneous analysis of four elements owing to hollow cathode lamp intensity limitations. Reported detection limits were approximately an order of magnitude worse than those reported for commercially available AA instruments using electrothermal atomization in the single element mode of operation.

Alder et al. (*6*) employed a direct reader with their furnace to analyze up to 9 elements simultaneously in the absorption mode. An array of hollow cathode lamps was used as the light source. The direct reader electronics were replaced by a custom-designed analog circuit which generated peak area information. However, there were no provisions for compensating for nonspecific background absorption and source fluctuation noise. Detection limits were comparable to commercially available AA instruments using electrothermal atomization.

This paper describes the design, construction, and operation of a simultaneous multielement atomic absorption spectrometer which is based upon a high-intensity continuum primary source, a high-resolution, wavelength modulated direct reading echelle polychromator, and a high-speed computer data acquisition system. This instrument has been dubbed SIMAAC. A single element spectrometer based on the same optical principles, called CEWM-AA, has been described previously (*13–15*). SIMAAC overcomes many of the limitations of previous designs. Up to 16 elements may be measured simultaneously with either flame or furnace atomization. Each channel operates in true double-beam, background corrected mode. The purpose of this paper is to describe the optical design and the data acquisition hardware and to demonstrate that with SIMAAC it is possible to obtain simultaneous multielement data with a single furnace atomization without significant signal-to-noise loss compared to single-element operation.

EXPERIMENTAL

Equipment. A block diagram of SIMAAC is shown in Figure 1. One of the unique aspects of this system is that most of the components are commercially available and are used with little or no modification (Table I). Very little mechanical or electronic engineering is required to build this system. This is an "equipment intensive" rather than a "labor intensive" approach.

The primary light source is a 300-W Eimac xenon arc lamp. This lamp provides intense, approximately collimated continuum radiation over the entire 200 to 600 nm spectral range (*16*). Previous measurements have shown that the intensity of this lamp over a typical atomic absorption profile is actually greater than that of conventional hollow cathode lamps, even for the As and Se wavelengths below 200 nm (*15*).

The atomizer can be a conventional flame or graphite furnace device. For this work an unmodified Perkin-Elmer HGA-2100

0003-2700/79/0351-2007$01.00/0

Table I. Components List

component	manufacturer	cost
Eimac lamp (300 W, VIX-UV) and power supply (PS 300-1)	Varian Eimac Division, San Carlos, Calif.	1 500
Echelle polychromator (Spectraspan IIIa, 20-channel multielement capabilities), includes PMT	Spectrametrics, Inc., Andover, Mass.	26 000
torque motor (G-300 PD) and controller (CCX-101)	General Scanning, Inc., Watertown, Mass.	1 000
graphite furnace (HGA-2200) and power supply	Perkin-Elmer Corp., Norwalk, Conn.	5 500
11/34-VE DECLAB system, AA11-K digital-to-analog converter, FP11-A floating point processor, VT-55-FE graphite terminal, LA-11-PA LA 180 line printer	Digital Equipment Corp., Maynard, Mass.	47 000

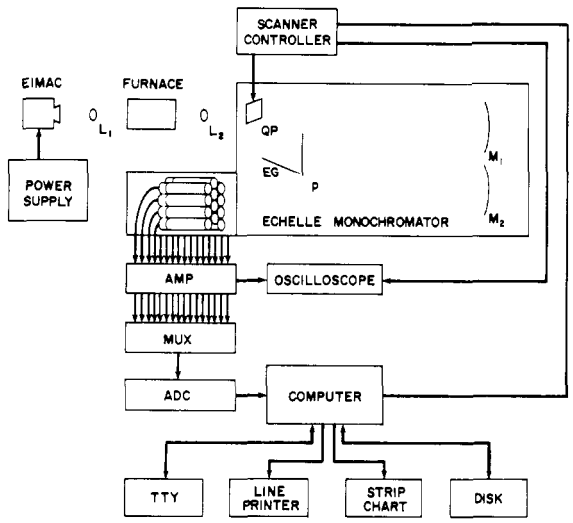

Figure 1. Block diagram of the SIMAAC system. L_1 and L_2, lenses. QP, quartz plate. EG, echelle grating. P, prism. M_1 and M_2, mirrors

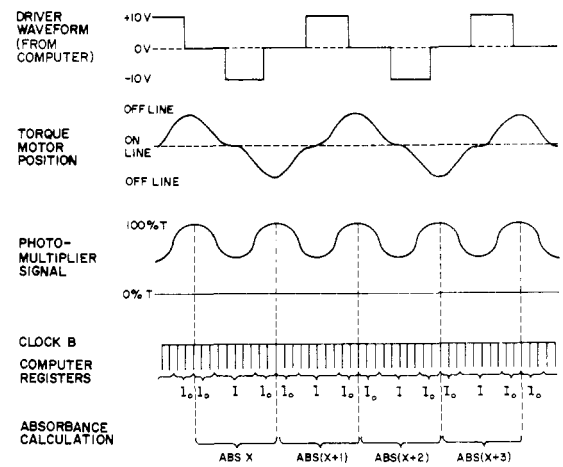

Figure 2. Timing scheme for wavelength modulation, data acquisition, and data reduction

graphite furnace has been used.

The spectrometer is a Spectraspan III Echelle polychrometer. This is a very compact 20-channel direct reader utilizing an echelle grating in conjunction with an order-separating prism. The echelle spectrometer focuses the dispersed spectrum as a two-dimensional array onto a removable mask or "cassette" in which the exit slits are located (*17*). In the single element mode, a single slit with conventional height and width controls is mounted in the cassette. For the multielement mode, up to 20 slits of a pre-specified height and width are appropriately positioned on the cassette face. Pinhead mirrors within the cassette direct the light from the slits to a fixed array of 20 end-on photomultiplier tubes. Once selected, the 20 slits cannot be relocated easily. However, the cassettes are easily changed, requiring only a few seconds to remove one and insert another.

Entrance and exit slit widths of 25 μm are used to obtain the resolution needed for good sensitivity and analytical curve linearity. Slit heights of 300 μm are used to reduce order-overlap stray light. The resulting small entrance slit area provides excellent rejection of atomizer emission, but unfortunately the reduced light throughput largely cancels the intensity advantage of the Eimac lamp.

The only modification which is made of the polychromator is to install a quartz refractor plate wavelength modulator as described previously for the single element system (*13*). The refractor plate is positioned just behind the entrance slit so that the entire spectrum at the focal plane can be modulated. The plate is mounted on an optical scanner torque motor. The motor has a position-sensing winding which provides an output voltage proportional to the actual refractor plate rotation angle (and thus to the wavelength displacement). It is possible, and often very useful, to observe the actual absorption profile, of one of the channels in real time by driving the x axis of an x-y oscilloscope from this position output and the y axis from the photomultiplier tube preamp output.

The cassette currently being used has exit slits positioned for the following elements and wavelengths: Ca (239.9 nm, 422.7 nm), Co (240.7 nm), Cr (357.9 nm), Cu (324.7 nm), Fe (248.3 nm, 302.1 nm), K (404.4 nm), Li (670.8 nm), Mg (202.5 nm, 285.2 nm), Mn (279.5 nm), Mo (313.3 nm), Na (330.3 nm, 589.6 nm), Ni (232.0 nm), Se (196.0 nm), Sn (224.6 nm), V (318.5 nm), and Zn (213.9 nm). These elements were selected because of the interest in their concentration in food samples. For most elements, the most sensitive resonance lines are used, but for those elements for which highly variable concentrations are anticipated (Ca, Fe, Mg, and Na for our applications), a second, less sensitive line is also included to extend the analytical range of measurement. Only the less sensitive 404.4-nm line of potassium is used, because of the anticipated high concentration of this element in most foods.

The photoanodic current from each photomultiplier tube is amplified by a simple preamplifier circuit consisting of a current-to-voltage converter and a non-inverting amplifier. This circuit is the only component of the system which was not obtained commercially. The gain of each preamp and the high voltage supply of each phototube is individually adjusted so that the preamp outputs are all close to 10 V when no absorption occurs. This ensures that the full range of the analog-to-digital converter (ADC) is utilized for each channel.

Data Acquisition. Data are acquired from the preamp outputs (at the rate of approximately 1000 readings per second per channel) by means of a minicomputer-based data system consisting of a PDP 11/34 equipped with a 16-channel multiplexer, a 12-bit (0–10.24 V) analog-to-digital converter (AD11-K), a 4-channel, 12-bit (-10 V to +10 V) digital-to-analog converter (AA11-K), a dual programmable real time clock (KW11-K), a general purpose, digital, 16-bit input/output interface (DR11-K), and a disk drive controller (RK11-D). Mass storage consists of two RK05 disks (1.25 million words each); one fixed and one removable cartridge. Communication with the system is accomplished with a VT55 decscope (terminal and graphic display and an LA180 line printer. The RT-11 (version 3) operating system is used.

The time relationship between the wavelength modulation and the sampling of intensity data from any *one* of the 16 channels is shown in Figure 2. The computer drives the scanner motor controller through one of its digital-to-analog converters. The modulation waveform is the 3-stepped waveform shown at the top of Figure 2. The middle step is centered on the atomic line of interest so that intensity readings can be made on the line and off the line on both sides. During each half-cycle of the modulation waveform the computer takes five readings of the signal voltage on the line and five readings of the line for each of the 16 channels.

Each set of ten readings for any one channel defines one point on the absorbance–time curve of that channel.

An assembly language program is used for data acquisition to meet the following modulation frequency and sampling rate requirements.

(1) The frequency of wavelength modulation must be sufficiently high to avoid the $1/f$ source flicker noise of the Eimac lamp which has been observed below 50 Hz (*16*). In this work the wavelength is modulated at 56 Hz, using the "stepped" waveform. With this waveform, the intensity modulation produced by an atomic line in the center of modulation interval occurs at twice the frequency of wavelength modulation, i.e., at 112 Hz in this case, well above the $1/f$ noise region.

(2) The period of modulation should be much smaller than the duration of the shortest absorption transient anticipated. With the HGA-2100 atomizer operated near its maximum temperature, volatile elements such as Zn and Pb produce absorption pulses with a duration of 0.2 to 0.5 s. Thus, the 112-Hz modulation frequency provides adequate time resolution.

(3) The sampling rate should be as high as possible so that each value of I_0 and I can be calculated from the largest possible number of ADC readings. This will help to reduce the effect of ADC quantization noise. The maximum sampling rate is limited by the ADC conversion time and the software overhead required to increment the multiplexer channel, to move the data from the ADC buffer to the data buffer, and to count conversions. For this work an overall sampling rate of 20.8 kHz is used. The sampling is multiplexed so that the 16 channels are read sequentially, which results in a channel sampling rate of 1.12 kHz per channel for each of the channels. This allows five readings each of I_0 and I on each channel during each half-period of the wavelength modulation waveform.

(4) Because of the high data rate, it is impossible to compute absorbance in real time from the intensity data. Therefore, the raw data are stored without processing during the atomization and are processed during the interval between atomizations when the furnace is cooling down and drying and ashing the next sample.

(5) A typical furnace atomization duration is 10 s. Within that period, a total of approximately 200 000 bytes of raw data will be accumulated from all 16 channels. Since this is much larger than the read–write memory capacity of the minicomputer, these data are stored on the RK05 high-speed hard disk as they are accumulated during the atomization. The disk controller hardware allows disk transfers to be accomplished without processor intervention once initiated.

Data Processing. The processing of the raw intensity data from each atomization is performed in the time interval between atomizations when the atomizer is cooling down and then drying and ashing the next sample. These steps normally take 1–2 min.

The essential data processing requirements can be broken down into three steps.

(1) Computation of a separate absorbance–time array for each channel from the raw intensity data for that channel.

(2) Measurement of peak area and/or peak height.

(3) Construction and use of analytical curves in the computation of analytical concentrations.

At the time of this writing, the data processing software was in a rather primitive state of development and only the first of these steps was implemented. This is sufficient, however, to demonstrate the signal-to-noise properties of the system. The program is written in FORTRAN with assembly language subroutines to access the raw data on disk. The data are processed one channel at a time according to the scheme shown at the bottom of Figure 2. During each half-cycle of the modulation waveform, ten intensity readings have been taken, five on the line and five off. Five intensity readings which were taken off the line are added up and the sum is called I_0. Five readings which were taken on the line are added up and called I. The program is written to account for the time delay (phase lag) between the applied torque motor driver waveform and the actual wavelength modulation waveform. Note also that the five readings which constitute one measurement of I_0 are split up into two groups of $2^1/_2$ values each before and after a group of I values. This is necessary to reduce the effect of rapid changes in I_0 with time which occur due to the transient background and light scattering from samples with complex matrices. Absorbance is then calculated as the common log of the ratio of I_0 to I. In this way, one value of absorbance is calculated for every half-cycle of the modulation waveform, i.e., for every ten intensity headings. Approximately 112 absorbances are computed per second per channel. These absorbance values are stored as a one-dimensional array for further processing. The absorbance arrays for the other channels are obtained in the same way. For demonstration purposes, any of the absorbance arrays can be output at a controlled rate via one of the 12-bit digital-to-analog converters for recording on a strip-chart recorder. This produces the kind of tracing which will be familiar to users of commercial single-element AA equipment. However, this mode of output would not ordinarily be used in routine multielement analysis; rather, peak area integrations (or possibly peak height measurements) will be made on the absorbance arrays directly.

Once the absorbance arrays have been calculated, it may be desirable to discard the original raw data; the absorbance arrays take only one-tenth the space in main memory or on disk as the raw data. On the other hand, there may be situations in which additional useful information may be able to be extracted from the raw data. For example, it would be easy to obtain a plot of background absorption vs. time. If a triangular wavelength modulation waveform is used, it would even be possible to observe the spectrum of the absorbing sample within the modulation interval at any point in the atomization period. Even though the sampling rate is only 20 points per modulation cycle (i.e., 10 points per spectral scan through the modulation interval), this should be sufficient to reveal the presence of structured background and line overlap with matrix absorption lines which might otherwise go unnoticed. Thus it may be advantageous to save the raw data even after the absorbance arrays have been computed. The maximum number of atomizations that can be collected before processing must occur is dependent on the number of cylinders of data collected for each analysis and the number of available empty removable disk cartridges. A sampling frequency of 1.12 kHz per channel requires one cylinder to store 5.5 s of data for each channel. Thus 30 cylinders are required if 16 elements are determined during a typical analysis where 10 s of data are recorded. This allows six atomizations to be recorded on a single disk cartridge. In routine work, however, the raw data on disk is reduced immediately after the atomization and is writtern over by the raw data from the next atomization.

RESULTS AND DISCUSSION

Noise Sources. Bower and Ingle (*18*) have done a very thorough analysis of the noise sources in atomic absorption spectrometry. In the SIMAAC system we expect the major noise sources to be photon shot noise at low concentrations and analyte absorption fluctuation noise at higher concentrations. Lamp fluctuation noise and background absorption fluctuation noise are expected to be reduced or eliminated by the wavelength modulation and ratio calculation. Atomizer background emission noise and analyte emission noise are expected to be reduced by the comparatively high brightness of the Eimac lamp and the comparatively small entrance slit area of the echelle polychromator. In the presence of high background (matrix) absorption, electronic noises are expected to become important.

The noise characteristics of SIMAAC were studied by measuring four different signals as a function of wavelength and/or source intensity. These four signals were: the electronic noise, σ_E (σ'_{ot} according to the convention of Bower and Ingle, ref. 18); the electronic noise with the furnace in the atomization cycle (σ_{ot}); and the I_0 noise, σ_{I_0} (σ'_{rt}) measured with and without wavelength modulation.

The electronic noise, σ_E, was measured with the Eimac lamp and the graphite furnace off. The major components are amplifier noise, ADC digitization noise, and photomultiplier tube (PMT) dark current noise. The noise contributed by the amplifier and the PMT dark current varies between elements depending on the amplifier gain and the PMT voltage. The digitization noise is constant for all channels, 0.72 mV, as determined by the magnitude of the quantization level of the 12-bit ADC, 2.4 mV (*19*). The electronic noise

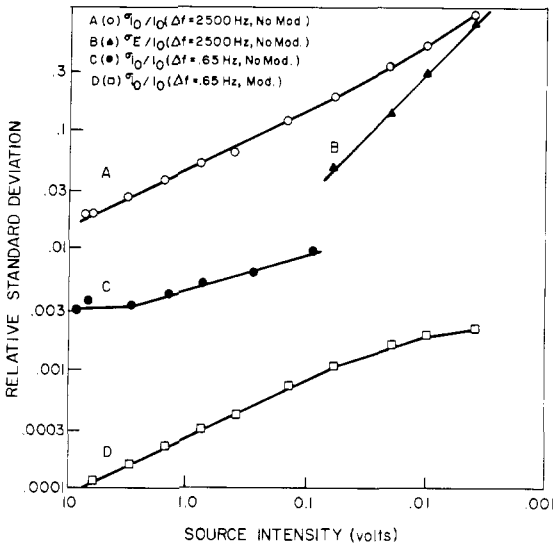

Figure 3. Relative standard deviation of measurement of photosignal as a function of intensity of I_0 expressed as output voltage of phototube preamplifier. (A) I_0 noise, 2500-Hz bandwidth, no wavelength modulation; (B) electronic noise only, same conditions as A; (C) I_0 noise, 0.65-Hz bandwidth, no wavelength modulation; (D) I_0 noise, 0.65-Hz bandwidth, with wavelength modulation

was measured simultaneously for eight channels using the data acquisition scheme described in the Experimental section (the PMT signal for each element is sampled at 1.12 kHz). σ_E was calculated from the standard deviation of ten signal measurements, each the average of 3840 ADC readings. For a combined analog–digital system the noise bandwidth, Δf, has been defined (*5*) as $1/(4\tau n)$ where τ is the standard analog RC filter time constant and n is the number of analog-to-digital conversions averaged. It is assumed that at least 2τ is allowed between conversions of the same signal to ensure that the two values are independent of each other. For SIMAAC, τ = 0.1 ms for the PMT–ADC interface circuit and each signal is measured every millisecond. Consequently, for n = 3840 the noise bandwidth for each determination is 0.65 Hz.

Since the electronic noise is constant for a given set of parameters, the relative electronic noise σ_E/I_0 will vary inversely with the source intensity. This is shown in Figure 3 for Cr (357.9 nm).

The electronic noise was also measured with the Eimac lamp off and the graphite furnace on, to determine the effect of furnace emission noise. With the furnace on, the noise levels ranged from comparable to 50% larger than the previously measured electronic noise. The increased noise levels were observed for elements with high PMT voltages and amplifier gains. The emission signal, along with the PMT dark current (the interface circuit is zeroed with current-to-voltage collector open), act analogous to stray light. The effect on the absorbance signal is minimal until high source attenuation (background absorbance of 2.0 or higher) occurs.

The I_0 noise, σ_{I_0}, was determined with the Eimac lamp on and the graphite furnace off. The I_0 noise is composed of electronic noise, photon shot noise, and lamp flicker noise. To emphasize the advantages of wavelength modulation in minimizing the flicker component, the I_0 noise was measured in two different modes.

The first approach was to measure I_0 noise in transmittance units as a function of I_0, without wavelength modulation. This was done at two noise bandwidths. Initially σ_{I_0} was determined from 768 analog-to-digital conversions ($\Delta f = 1/4\tau n$ = 2500 Hz, where τ = 0.1 ms and n = 1). As shown for Cr (357.0 nm) in Figure 3, plot A, the log of σ_{I_0}/I_0 has a slope of –0.47 as a function of the log of I_0. This slope closely approximates that of a shot noise limited system (–0.5), despite the presence of the Eimac flicker noise which has been documented by Cochran and Hieftje (*16*). The minimal influence of the flicker noise is a consequence of the large noise bandwidth. Next, σ_{I_0} was computed from 10 values, each of which was the average of 3840 conversions (Δf = 0.65 Hz where τ = 0.1 ms and n = 3840). At this lower bandwidth, lamp flicker noise is expected to become more important, because the $1/f$ component of the flicker noise is not much reduced by the reduced bandwidth, whereas the white shot noise decreases proportionally with the square root of bandwidth. For this case, Δf = 0.65, the log of σ_{I_0}/I_0 gives a maximum slope of –0.29 (Figure 3, plot D) as a function of the log of I_0. At high source intensities, the slope approaches zero, as would be expected if source flicker noise becomes dominant. Thus the source flicker noise is important at lower bandwidths.

The second approach was to calculate σ_{I_0}/I_0 from the absorbance base-line noise with wavelength modulation ($\sigma_{I_0}/I_0 = \sigma_A/0.43$). Absorbance values are computed at a frequency of 112 Hz. Cochran and Hieftje (*16*) have shown that the $1/f$ component of the Eimac flicker noise is observed at frequencies below 40–50 Hz. Consequently, compensation for this $1/f$ component is expected. This was verified experimentally as shown for Cr (357.9 nm) in Figure 3, plot B. σ_A was determined from 10 values each of which was the result of 3840 conversions (Δf = 0.65 Hz). The slope of the log of σ_{I_0}/I_0 as a function of the log of I_0 is –0.5. These results indicate that the lamp flicker noise is predominately of low-frequency ($1/f$) character and that wavelength modulation successfully compensates for this component of noise.

All the elements measured showed noise responses similar to Cr (Figure 3). Each element had a slope of –0.5 when the log of the base-line absorbance noise was plotted as a function of the log of the source intensity. The plots were offset vertically depending on whether the Eimac was more or less intense than at the Cr wavelength (357.9 nm). Thus SIMAAC is shot noise limited for all elements near the detection limit. As analyte absorbance increases, analyte concentration fluctuation noise will become dominant. Near the detection limit, the shot noise limited case persists until the source attenuation, which would occur for high salt samples, reaches the point where electronic noise becomes significant. For Cr (357.9 nm) this transition occurs after the source has been attenuated by a factor of 250 whereas for Zn (213.9 nm), at which wavelength the Eimac is much less intense, the transition occurs after 70-fold attenuation of the source.

As will be shown later in the paper, SIMAAC sensitivities are comparable to conventional AAS sensitivities. Consequently, a comparison of SIMAAC noise levels to those of other systems is informative. Table II compares the electronic and I_0 noise of SIMAAC, another multielement AAS (*20*), and a Varian Techtron AA-6 (*18*). For SIMAAC, σ_{I_0}/I_0 computed from base-line absorbance noise, this comparison shows the expected wavelength dependence. The Eimac lamp has a maximum intensity at 500 nm and is almost three orders of magnitude less intense at 198 nm. SIMAAC shows comparable noise levels around 280 nm, lower noise levels at higher wavelengths, and higher noise levels at lower wavelengths. This trend is identical to that observed in earlier studies where the photon flux at the photodetector was compared for the Eimac–echelle system and a typical line-source system consisting of a hollow cathode lamp (HCL) and a 0.5-m Ebert monochromator (*15*). As a result, one expects SIMAAC to have detection limits equal to or better than those of line-source AAS for elements above 280 nm and poorer detection limits below 280 nm. However, because of the square-root relationship between photon shot noise and intensity, the degradation in detection limits at shorter wavelengths is

Table II. Comparison of System Noise Sources[a]

element	wavelength, nm	I_o noise, % SIMAAC[b]	I_o noise, % TMMS[c]	I_o noise, % V[d]	electronic noise, %[e] SIMAAC	electronic noise, %[e] TMMS[3]	throughput ratios:[f] Eimac-echelle vs. HCl-0.5-m Ebert monochromator
Zn	213.9	0.21	0.12	0.09	0.012	0.014	0.09
Sn	224.6	0.24	--	--	--	--	--
Cd	228.8	--	0.04	0.05	--	0.015	0.25
Ni	232.0	0.16	0.05	0.15	0.005	0.03	0.11
Mn	279.5	0.04	0.05	0.04	0.004	0.03	0.23
Pb	283.3	--	0.05	--	--	0.01	0.16
Mg	285.2	0.05	0.05	0.04	0.007	0.006	1.7
Fe	302.1	0.05	--	--	0.006	--	2.5
Cu	324.7	0.04	0.07	0.05	0.002	0.007	1.4
Cr	357.9	0.02	--	--	0.002	--	2.2
Ca	422.6	0.02	--	--	0.003	--	4.9
Na	589.6	0.02	--	--	0.004	--	--

[a] σ_{I_o}/I_o (or σ'_{rt}/E'_r by convention of Bower and Ingle, ref 18) × 100%. [b] $\sigma_{I_o}/I_o = \sigma_A/0.43$. [c] Time, Multiplex Multiple Slit Multielement Flame AAS (*20*). [d] Varian Techtron, AA-5 (*8*). [e] σ_E/I_o (or σ_{ot}/E'_r by convention of Bower and Ingle, ref 18) × 100%. [f] Ref. 15.

modest and in most cases is less than the uncertainty in measuring the detection limits.

S/N Ratio Comparison: Multielement vs. Single Element Measurements. A comparison of the signal-to-noise ratios between the single element, analog CEWM-AA and the multielement, digital SIMAAC will reveal any loss in capabilities associated with the conversion from the single element to the multielement analytical mode. A degradation of the analytical capabilities can arise from three possible sources: (1) The difference in optical paths (the multielement vs. the single element exit slit cassettes); (2) the difference in the data acquisition systems (high frequency multiplexed digital sampling vs. continuous analog measurement); and (3) the use of compromise analytical conditions for multielement analyses.

The variation in the optical paths between single element and multielement operation lies in the use of the multielement exit cassette. Significant differences in signal intensity absorbance can arise for several reasons. First, the multielement cassette uses pin-head mirrors for all but five elements (Se 196.0 nm, Sn 224.6 nm, Ca 239.8 nm, V 318.5 nm, and Na 330.2 nm) to reflect the light from the exit slits to the appropriate PMT. Spectrametrics has reported a 25% loss in intensity as a result of these mirrors (*21*). With a shot noise limited system, this corresponds to a 13.4% decrease in the signal-to-noise ratio. This degradation has not been experimentally verified.

Ideally, the focal plane of the echelle is flat and superimposed on the plane of the exit cassette. If not, then poorer resolution and decreased analytical sensitivity (increased characteristic concentration) will be observed for at least some of the channels. The data in Table III allow the resolution of the single element and multielement modes to be compared. In each case, the full width at half height (fwhh) was determined for hollow cathode lamp emission lines using a mechanical scanning device. In general, the resolution in the multielement mode is comparable to that of the single element mode; however, a trend is visible. Resolution in the multielement mode becomes comparatively worse at higher wavelengths.

Finally, in order to have maximum sensitivity for all elements simultaneously, the exit slits on the multielement cassette must be aligned such that they all rest on their respective absorption peaks at the same time. The overall alignment of the spectrum at the focal plane with respect to the exit slit cassette can be controlled by the operator from the front panel wavelength controls and can be fine tuned at any time if necessary. The internal alignment of one exit slit with respect to the others is set when the cassette is manufactured and cannot be modified by the user. This alignment is performed adequately by the manufacturer of the echelle spectrometer. Wavelength drift has not been observed to be a significant factor.

Table III. Comparison of Single Element and Multielement Mode Resolution

element	wavelengths, nm	fwhh, nm[a] single element	fwhh, nm[a] multielement	resolution, nm[b]
Zn	213.8	0.0024	0.0023	0.0019
Ca	239.8	0.0033	0.0023	0.0022
Mn	279.5	0.0039	0.0038	0.0026
Mg	295.2	0.0041	0.0027	0.0027
Fe	302.1	0.0042	0.0046	0.0029
Na	330.2	0.0046	0.0053	0.0032
Cr	357.9	-	0.0058	0.0036
Ca	422.6	0.0056	0.0070	0.0043
Na	589.6	0.0085	0.0151	0.0066

[a] Experimental data using mechanical scanning, 25-μm wide entrance and exit slits. [b] Ref. 35, 25-μm entrance and exit slits.

The data acquisition systems of the two modes are drastically different. In the single element mode, absorbance is computed continuously by an analog circuit (*14*). [This operational amplifier circuit simultaneously determines I_o and I which are input to a log ratio module, providing a continuous absorbance output.] In the multielement mode, the absorbance is computed digitally as described in the Experimental section at the rate of 112 computations per second. The signal-to-noise ratios of the two methods were compared for the graphite furnace measurement of a 50-ppb Pb standard. Representative traces are shown in Figure 4. Due to the rapid rate of absorbance calculation in the digital system, the effective electrical bandwidth of the digital system is much greater than that of the analog system. Consequently, a larger signal and a larger noise component are observed. The digital data acquisition system resulted in a 14% loss in the signal-to-noise ratio when sine wave modulation was used.

The use of the computer to drive the torque motor controller provides more freedom in selecting the modulation waveform (22). With analog circuitry, it is difficult to obtain any response from the torque motor other than a sine wave when frequencies greater than 50 Hz are used. The sinusoidal response of the torque motor results in the PMT signal being a distorted sine wave. The computer-generated three-step square wave (Figure 2) produces a PMT signal which is closer to a square wave. Consequently, the result is an increase in

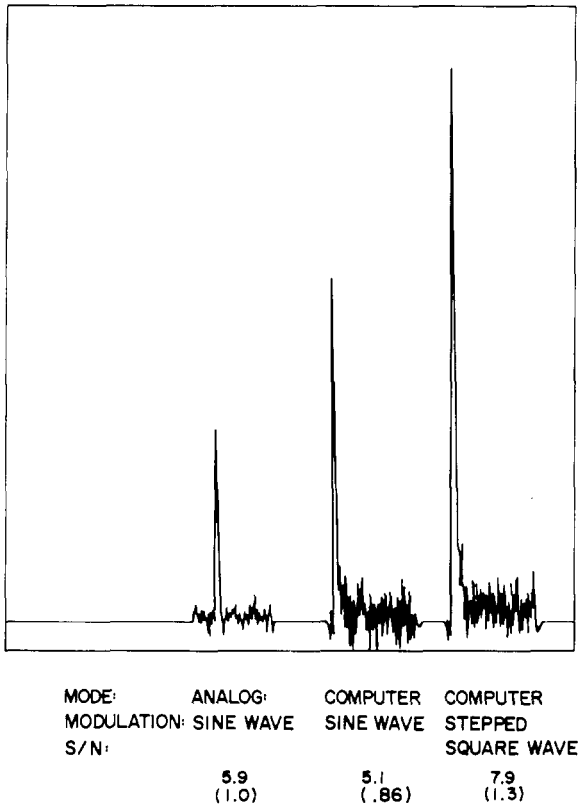

Figure 4. Comparison of signal-to-noise ratios for analog and digital data acquisition and for sine and stepped square wave modulation

the signal as shown in Figure 4; the added versatility in generating the modulation waveform results in a net improvement of 30% in the signal-to-noise ratio for the multielement system.

In the single element mode, it is possible to optimize all instrumental parameters for the element being analyzed. For multielement analyses, though, it becomes necessary to select parameters which are either average values for the elements being analyzed or extreme values in order to protect the analytical integrity of one or more of the elements. These non-optimal, or compromise, analytical conditions result in reduced signal-to-noise ratios for some elements.

For the SIMAAC system, relatively few compromises are necessary. The Eimac lamp is run at a near maximum current of 20 A. Unlike conventional AA systems where sensitivity is reduced at high hollow cathode lamp currents due to self absorption of the emission line, SIMAAC detection limits improve proportionally with the square root of the source intensity. Consequently, a maximum operating current for the Eimac is optimal for all elements.

Furnace atomization conditions are dictated by the elements being analyzed. The atomization temperature must be high enough that even the least volatile element is volatilized. The ashing temperature must be low enough that the most volatile element is not volatilized prematurely. Drying conditions are assigned to provide gentle evaporation of the solvent without scattering the sample about the interior of the furnace.

Three parameters on the echelle monochromator are variable: the entrance slit height and width (all exit slits were specified to be 25 μm wide and 300 μm high when the multielement cassette was ordered), and the modulation interval. The best resolution available is necessary to obtain maximum sensitivity for SIMAAC or CEWM-AAS. Consequently, 25-μm wide entrance and exit slits are routinely used. Slit heights of 300 μm are used as a compromise between intensity and order-overlap stray light (*13*). Optimum refractor plate modulation angles range from ±3° to ±5° using

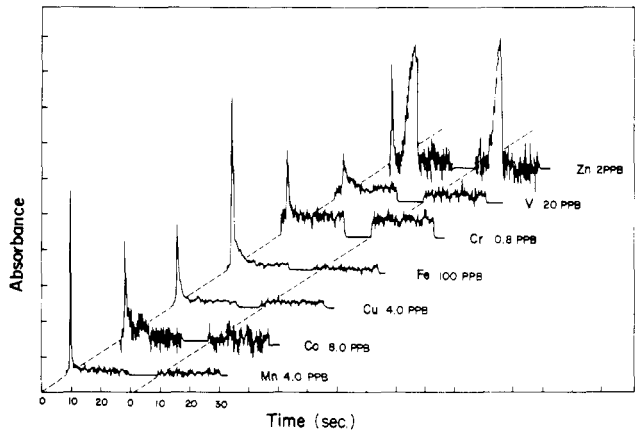

Figure 5. Simultaneous furnace atomizations for a mixed standard followed by a blank solution

a sine wave. (The corresponding wavelength modulation interval in nanometers varies with the dispersion of the monochromator.) With stepped square wave modulation, the amplitude is less critical and is slightly larger. Consequently, little change in sensitivity is expected with a modulation angle of ±6°.

The combined effect of all three factors, the optical path, the data acquisition system, and the compromise analytical conditions, is determined by comparing simultaneous multielement detection limits with those obtained in the single element mode. The simultaneous multielement detection limits were obtained using the following parameters: a 20-A Eimac lamp current, a 20-s dry cycle with the temperature ramped from ambient to 150 °C, a 10-A ash at 300 °C, and 8-s atomization at 2800 °C, (all temperatures as read from HGA-2100 power supply), entrance slits of 25 μm × 300 μm, Ar sweep gas in the interrupt mode, and a modulation angle of ±6°. The results shown in Table III indicate that the detection limits for SIMAAC and CEWM-AAS do not differ significantly compared with the variation associated with individual run conditions. A systematic study of the effect of the compromise analytical conditions (furnace temperatures, modulation interval, modulation waveform, and slit function) on sensitivity and detection limits has begun but is beyond the scope of this paper.

Multielement Measurements. The absorbance–time traces for the simultaneous atomization of the seven elements listed in the previous section are shown in Figure 5. The traces show the atomization of a mixed standard in a dilute HNO_3 solution followed by a dilute acid blank. The absorbance time arrays were read out individually to a strip chart recorder by a digital-to-analog converter. A software time delay was incorporated into the output routine so that the absorbance arrays would be recorded at the same rate as they occurred in real time. No damping was used for the read-out other than that inherent in the response time of the strip chart recorder. Each trace lasts approximately 20 s and contains 2300 absorbance points. A different vertical scale expansion has been used for each trace to emphasize the signal-to-noise ratio.

For these studies an extremely volatile element, Zn, and an extremely nonvolatile element, V, were included. These elements represent the extremes in atomization conditions. The atomization temperature was chosen to optimize the V signal, while a minimal ashing temperature was chosen so as not to volatilize the Zn prematurely. The high atomization temperature did not result in a smaller peak height (than observed at lower temperatures) for any of the elements. The only unusual aspect of the traces is the residual peak for Zn. This peak persisted regardless of whether a blank or a dry

Table IV. Absolute Detection Limits (pg) (Standard Resonance Wavelengths Except Where Noted)

element	SIMAAC[a] (multielement)	CEWM-AAS[a] (single element)	conventional-AAS[b] (single element)	ICP-AES[c] (multielement)
Ba	-	3[d]	15	7.5-20[e]
Cd	-	1-4	0.1-0.5	63-400
Co	14-16	-	4-10	90-400[f]
Cr	1.5-2.0	0.6-2	1-5	72-200[f]
Cu	2.5-6.0	6-12	1-20	36-200
Fe	23-50[e]	50[e]	2-3	68-400[f]
Mg	0.8	0.8	0.4	2.2-200[f]
Mn	1-4	2-4	1	9-40[f]
Pb	-	20-28	5-6	900-4000[f]
V	49-58	-	8-360	45-200[f]
Zn	2-6	2-3	0.1-2.7	45-200

[a] This work; 20-μL sample size; range of values reflects uncertainty of detection limit determination and long-term variation in sensitivity due to normal variations in experimental conditions. [b] Ref. 23-25; 5-100 μL sample sizes; range reflects extremes of listed values. [c] The first figure shown in the best published detection limit using ultrasonic nebulization-desolvation and the second figure is that for pneumatic nebulization (*28, 29*) using 750-μL and 200-μL sample sizes, respectively. [d] Ref. 36; 20-μL sample size. [e] 302.0-nm wavelength. [f] Analytical wavelengths are nonresonance lines chosen for greater sensitivity.

Table V. Absolute Characteristic Concentrations (pg)[a]

element	SIMAAC[b]	Perkin-Elmer[c]
Co (240.7)	13-15	44
Cr (357.9)	10-13	10
Cu (324.7)	9-21	22
Fe (302.0)	120-260	--
(248.3)	---	30
Mg (285.2)	3	3
Mn (279.5)	2-8	5
V (318.5)	350-410	400
Zn (213.9)	1-3	1

[a] Analyte in pg necessary to give 0.0044 absorbance. [b] This work. [c] Ref. 24.

rod was analyzed and persisted upon replacement of the graphite rod and end cones. It is suspected that the residual peak is due to Zn contamination somewhere in the surrounding atomizer body. The data reduction software ignores this peak.

The absolute detection limits and characteristic concentrations listed in Tables IV and V, respectively, were calculated from the absorbance vs. time traces in Figure 5 and traces of similar determinations. The absolute detection limit is defined as the amount of analyte, based on a 20-μL sample, for which the signal is twice the RMS noise of the base line. The noise levels were measured just off the analytical line. The peak height method was used to calculate detection limits to conform with previous determinations. The absolute characteristic concentration is the amount of sample necessary to give an absorbance of 0.0044.

SIMAAC characteristic concentrations are comparable to those listed by Perkin-Elmer for the HGA-2100 with the exception of Fe which is approximately a factor of four worse. The Fe line at 302.0 nm is used for SIMAAC because although both lines (302.0 and 248.3 nm) give the same characteristic concentration, the lower noise levels at 302.0 nm (because of higher Eimac intensity) result in better detection limits.

A comparison of detection limits for SIMAAC, CEWM-AAS, commercially available line-source AAS using electrothermal atomization, and induction-coupled plasma atomic emission spectrometry (ICP-AES) is shown in Table IV. The range of values listed for SIMAAC and CEWM-AAS reflects the day-to-day variability of this parameter. The noise component, which is dependent on the intensity of the Eimac lamp, remained stable. However, the sensitivity varied considerably (Table V) depending on individual furnace characteristics, the fitting of the furnace tube to the end cones, the flow rate of the cooling water, and a number of other variables. Consequently a range of detection limits is more realistic than a single value for each element.

The range of values listed for commercially available AA systems reflects the range of detection limits reported in the three references (*23–25*). None of these detection limits were obtained using background correction, which can result in a factor of 2 to 4 deterioration in the S/N ratio (*26, 27*). The comparison to ICP-AES detection limits is complicated by the fact that the latter are normally reported in concentration units, while furnace detection limits are usually reported in absolute mass units. Thus the solution volume requirements for ICP-AES must be considered.

The two values listed for ICP-AES are calculated from the best reported concentration detection limits for ultrasonic and penumatic nebulization, respectively (*28, 29*). These detection limits were acquired using 16–20 s integration times with a sample uptake rate of 2.5 to 3 mL. Thus, 750 to 900 μL of sample were used. However, Fassel and Kniseley (*30*) found that 200 μL was sufficient for the determination of state-of-the-art ICP detection limits using penumatic nebulization. Use of 25-μL sample sizes for pneumatic nebulization had been reported previously (*31*), but it was acknowledged that detection limits improved by a factor of 5 when 150–200 μL sample sizes were used. To the best knowledge of the authors, aspiration of microsamples by ultrasonic nebulization has not been reported for use with ICP-AES. As a result, the absolute detection limits listed in Table IV for ICP-AES were determined from the best reported detection limits with ultrasonic and pneumatic nebulization using a 750-μL and 200-μL sample size, respectively.

SIMAAC detection limits compare well with those listed for CEWM-AAS and commercially available AAS. Both SIMAAC and CEWM-AAS have detection limits for Zn (2–6 pg and 2–3 pg, respectively) which are an order of magnitude worse than those listed by Perkin-Elmer for the HGA-2100 0.1 pg). This is at least partly due to the low intensity of the Eimac lamp in the UV region. However, the SIMAAC and CEWM-AAS detection limits for Zn agree well with that determined by Sturgeon et al. (*23*) using the same furnace with a commercially available line source AAS. For the elements reported here, SIMAAC detection limits are comparable to an order of magnitude better than ICP-AES absolute detection limits using ultrasonic nebulization and desolvation. Using pneumatic nebulization, ICP-AES is one to three orders of magnitude worse. (The *concentration* detection limits of SIMAAC, assuming a 20-μL sample size are roughly comparable to those reported for ICP-AES with pneumatic nebulization using a much larger sample size.)

It became obvious with these studies that integration of the peak area offers significant advantages for the simplification

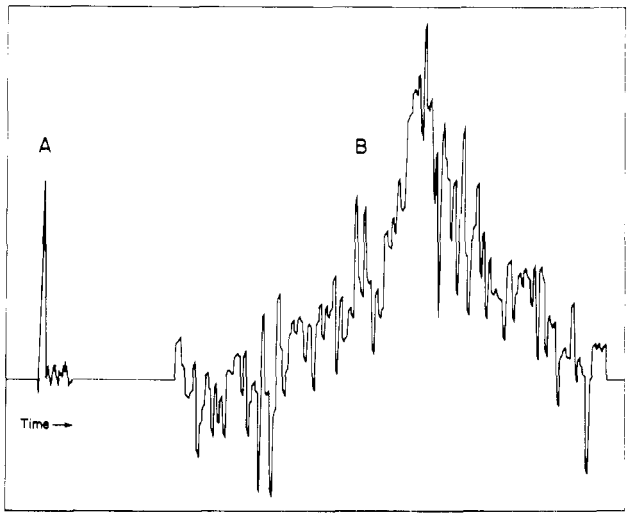

Figure 6. Trace of the determination of ppb Zn; (A) plotted at a rate corresponding to a real-time absorbance read-out, and (B) plotted at a rate 60 times slower to allow individual points to be seen

of the data processing as well as for the measurement of analytical signals. The advantages of integration can be seen by taking a closer look at a typical absorbance–time array. The traces for the analysis of 5 ppb Zn are shown in Figure 6 as plotted by the computer. The traces on the left show the data plotted at a rate corresponding to real-time absorbance read-out. The traces on the right show the same data plotted at a rate 60 times slower, allowing the individual absorbance points to be seen without the low-pass filtering effect of the strip chart recorder. The arrays plotted at a slowed rate show that there is a great deal of uncertainty as to the true peak height. Qualitative information regarding the absorbance peak shape can be better obtained by using a numerical smoothing technique (*32*, *33*). Quantitatively, the simplest approach is to integrate the absorbance values over the peak. From the data processing point of view, integration of the peak can be performed very easily. The absorbance points are simply summed over a predetermined interval optimized for each element. Sturgeon et al. (*23*) have reported as much as a factor of two increase in the linear range of the analytical calibration curves using integration of the peak area. A similar increase in the linear range of the working curves has also been observed in our work. Analytical calibration curves for SIMAAC, based on peak height measurements, are linear (slope of one on a log–log plot) for one to two orders of magnitude of concentration. The linearity of analytical curves based on peak area is increased by approximately one half an order of magnitude of concentration using a fixed integration interval which was not specifically optimized for each element or for the concentration range measured.

In spite of the limited linear range, the measured absorbance continues to increase monotonically with concentration for three or more orders of magnitude of concentration. The ability to use the analytical curves in the nonlinear region will depend on the reproducibility of the curves and on the availability of suitable curve fitting algorithms. This aspect has not yet been investigated. In some cases it may be desirable to devote some of the channels to less sensitive absorption lines as has been done with the multielement cassette described here for Na, Ca, Mg, and Fe. This is another reason why a large number of channels is desirable; even if two lines are used for every element, it would still be possible to measure eight elements simultaneously. For this purpose, a secondary line with between one and three orders of magnitude less sensitivity is desirable. Of the elements which can be determined by atomic absorption only As, Be, Hg, and Zn do not have suitable secondary lines. A detailed consideration of the analytical curve shapes in SIMAAC will be the subject of a later paper.

The time resolution of SIMAAC is comparable to or better than most conventional AAS instruments. Under normal operating conditions, the SIMAAC samples each channel at a frequency of 1.12 kHz. As a result, 112 background corrected absorbance values are computed each second for each channel (Figure 4). Currently available analog, oscilloscope display systems offer only twofold better resolution for a single channel without background correction (*34*). From a qualitative point of view, the resolution of multielement CEWM-AAS appears to be sufficiently fast to allow characterization of the peak shape. The atomization of Zn at 2800 °C is close to a worst case test of the system response. The width of the 5 ppb Zn peak (Figure 6) was approximately 0.4 s, yet over 40 absorbance points have been computed in its duration.

LITERATURE CITED

(1) J. D. Winefordner, J. J. Fitzgerald, and N. Omenetto, *Appl. Spectrosc.*, **29**, 3 (1975).
(2) R. D. Ediger, W. B. Barnett, S. M. Gamache, and D. L. Wilson, Paper #220, 29th Pittsburgh Conference on Analytical Chemistry and Applied Spectroscopy, Cleveland, Ohio, 1978.
(3) R. Mavrodineanu and R. C. Hughes, *Appl. Opt.*, **7**, 1281 (1968).
(4) E. Lundberg and G. Johansson, *Anal. Chem.*, **48**, 1922 (1976).
(5) E. D. Salin and J. D. Ingle, Jr., *Appl. Spectrosc.*, **32**, 596 (1978).
(6) J. F. Alder, D. Alger, A. J. Samuel, and T. S. West, *Anal. Chim. Acta*, **87**, 301 (1976).
(7) N. Furuta, H. Haraguchi, and K. Fuwa, *Anal. Chem.*, **49**, 1263 (1977).
(8) A. Strasheim and Human, *Spectrochim. Acta, Part B*, **23**, 265 (1968).
(9) K. M. Aldous, D. G. Mitchell, and K. W. Jackson, *Anal. Chem.*, **47**, 1034 (1974).
(10) H. L. Felkel and H. L. Pardue, *Anal. Chem.*, **49**, 1112 (1977).
(11) G. Horlick and E. Codding, *Appl. Spectrosc.*, **29**, 167 (1975).
(12) D. G. Mitchell, K. W. Jackson, and K. M. Aldous, *Anal. Chem.*, **45**, 1215A (1972).
(13) A. T. Zander, T. C. O'Haver, and P. N. Keliher, *Anal. Chem.*, **48**, 1166 (1976).
(14) J. M. Harnly and T. C. O'Haver, *Anal. Chem.*, **49**, 2187 (1977).
(15) T. C. O'Haver, J. M. Harnly, and A. T. Zander, *Anal. Chem.*, **50**, 1218 (1978).
(16) R. L. Cochran and G. M. Hieftje, *Anal. Chem.*, **49**, 2040 (1977).
(17) P. N. Keliher, *Res./Dev.* **27**(6), 26 (1976).
(18) N. W. Bower and J. D. Ingle, Jr., *Anal.* Chem., **49** , 574 (1977).
(19) G. Horlick, *Anal. Chem.*, **47**, 352 (1975).
(20) E. D. Salin and J. D. Ingle, Jr., *Anal. Chem.*, **50**, 1745 (1978).
(21) Spectrametrics, Inc., Andover, Mass., personal communication, 1978.
(22) S. R. Koirtyohann, E. D. Glass, D. A. Yates, E. J. Hinderberger, and F. E. Lichte, *Anal. Chem.*, **49**, 1121 (1977).
(23) R. E. Sturgeon, C. L. Chakrabarti, and P. C. Bertels, *Anal. Chem.*, **47**, 1250 (1975).
(24) "Technique and Applications of Atomic Absorption", Perkin-Elmer Corp., Norwalk, Conn., Order No. AA-3226, March, 1978.
(25) C. Veillon, from "Trace Analysis", J. D. Winefordner, Ed., John Wiley and Sons, New York, 1976.
(26) W. B. Barnett and J. D. Kerber, *At. Absorp. Newsl.*, **13**, 56 (1974).
(27) E. Lundberg and G. Johansson, *Anal. Chem.*, **48**, 1922 (1976).
(28) V. A. Fassel and R. N. Kniseley, *Spectrochim. Acta, Part B*, **32**, 327 (1977).
(29) P. W. J. M. Boumans and F. J. de Boer, *Spectrochim. Acta, Part B*, **30**, 309 (1975); **32**, 365 (1977).
(30) V. A. Fassel and R. N. Kniseley, *Anal. Chem.*, **47**, 1110A (1975).
(31) R. N. Kniseley, V. A. Fassel, and C. C. Butler, *Clin. Chem. (Winston-Salem, N.C.)*, **19**, 807 (1973).
(32) A. Savitsky and M. L. E. Golay, *Anal. Chem.*, **36**, 1627 (1964).
(33) G. Horlick, *Anal. Chem.*, **47**, 352 (1975).
(34) L. P. Morganthaler, Paper #135, 29th Pittsburgh Conference on Analytical Chemistry and Applied Spectroscopy, Cleveland, Ohio 1978.
(35) C. C. Wohlers, Ph.D. Thesis, Villanova University, Villahova, Pa., 1975.
(36) J. D. Messman, M. S. Epstein, and T. C. Rains, National Bureau of Standards, Gaithersburg, Md., personal communication, 1978.

RECEIVED for review March 8, 1979. Accepted June 11, 1979.